

Multipole solitons in competing nonlinear media with an annular potential

Liangwei Dong ^{1,*} Mingjing Fan ² Changming Huang ³ and Boris A. Malomed ^{4,†}

¹*Department of Physics, Zhejiang University of Science and Technology, Hangzhou 310023, China*

²*Department of Physics, Shaanxi University of Science and Technology, Xi'an 710021, China*

³*Department of Electronic Information and Physics, Changzhi University, Changzhi, Shanxi 046011, China*

⁴*Instituto de Alta Investigacion, Universidad de Tarapaca, Casilla 7D, Arica, Chile*



(Received 18 September 2023; accepted 1 November 2023; published 1 December 2023)

We address the existence, stability, and propagation dynamics of multipole-mode solitons in cubic-quintic nonlinear media with an imprinted annular (ring-shaped) potential. The interplay of the competing nonlinearity with the potential enables the formation of a variety of solitons with complex structures, from dipole, quadrupole, and octupole solitons to necklace complexes. The system maintains two branches of soliton families with opposite slopes of the power-vs.-propagation-constant curves. While the solitons' stability domain slowly shrinks with the increase of even number n of lobes in the multipole patterns, it remains conspicuous even for $n > 16$. The application of a phase torque gives rise to stable rotation of the soliton complexes, as demonstrated by means of analytical and numerical methods.

DOI: [10.1103/PhysRevA.108.063501](https://doi.org/10.1103/PhysRevA.108.063501)

I. INTRODUCTION

Various types of self-bound states exist in diverse nonlinear systems [1–3]. Generic species of such states include dipole [4–6], quadrupole [6,7], and necklace solitons [8–12], as well as vortex solitons carrying angular momentum [13–15]. These are fundamentally important modes in nonlinear optics, Bose-Einstein condensates (BECs), plasmas, and so on.

In addition to the ubiquitous cubic (Kerr) nonlinearity, a variety of competing nonlinearities, aiming to arrest the two-dimensional (2D) critical collapse, driven by the cubic self-focusing, and thus stabilize 2D solitons, were proposed theoretically and observed experimentally [3]. Representative examples include quadratic-cubic [$\chi^{(2)} : \chi^{(3)}$] [16] and cubic-quintic [$\chi^{(3)} : \chi^{(5)}$, alias CQ] [17–19] optical media, where the focusing lower-order nonlinear term is necessary for self-trapping of the localized states, while the higher-order defocusing nonlinearity secures the arrest of the collapse. In this case, the nonlinear index of refraction is negative at the peak (center) of the self-trapped light beam, while remaining positive in the beam's wings. The dielectric response of some materials used in nonlinear optics is accurately approximated by the CQ combination of nonlinear terms [20,21]. Spatial optical solitons were also observed in a setting featuring quintic-septimal (focusing-defocusing) nonlinearities with negligible third-order nonlinearity [22]. Competing nonlinearities have also been studied in plasma physics [23], as well as in the context of Bose superfluids [24].

Multipole solitons feature a periodic azimuthal structure consisting of an even number n of lobes (poles), which are distributed evenly on a ring. Adjacent lobes have opposite

signs, hence n cannot be odd (except for $n = 1$, which corresponds to the axisymmetric ground-state mode). The simplest structured state is the dipole, which corresponds to $n = 2$. The thickness of the lobes is usually much smaller than the effective radius of the ring. Though the diffraction of multipole modes can be effectively stymied by the nonlinearity, the expansion in the radial direction [25] or spiral rotation [26] eventually destroys the patterns in the course of long propagation.

The concept of 2D multipole solitons was put forward in Refs. [27,28], where stabilization of multipole structures was achieved due to cross-phase-modulation coupling with a nodeless field in a two-component system. The existence of such solitons requires a focusing saturable nonlinearity. On the other hand, the expansion of necklace-like beams in focusing Kerr media can be slowed down by the angular momentum imprinted upon the pattern [29]. Another method for suppressing the expansion of necklace beams was elaborated in saturable systems with fractional diffraction [12]. Metastable necklace beams were also predicted in settings with competing quadratic-cubic [30] and cubic-quintic [8,31] nonlinearities and observed in local [32] and nonlocal nonlinear media [33].

Relevant alternatives for trapping stable multipole solitons are provided by confinement, with radial modulation of the local refractive index inducing an effective trapping potential [6,34]. Although local variation of the index is always small in comparison to its background value, the corresponding potential may be sufficient to strongly affect properties of nonlinear modes (in particular, to stabilize them). Multipole-mode solitons can be supported by different forms of photonic lattices (potentials) and various types of optical waveguides [35–47]. Particularly, multipole solitons may be made stable under appropriate conditions in passive [35,38–40] and \mathcal{PT} -symmetric lattices [42,43], circular waveguide arrays [44], and axially symmetric Bessel lattices [45–47].

*dlw_0@163.com

†On sabbatical leave from the Department of Physical Electronics, School of Electrical Engineering, Tel Aviv University, Tel Aviv, Israel.

In addition to multipole solitons in optics, patterns with different values of n were also predicted in BECs with contact [48] and dipole-dipole [49] interactions. In binary BECs, metastable quantum droplets in the form of ring-shaped clusters were constructed in systems modeled by the amended Gross-Pitaevskii equation with the Lee-Huang-Yang (beyond-mean-field) correction [50]. Stable multipole quantum droplets were predicted in a weakly anharmonic potential [51].

Though many efforts were put forth to suppress the instability of multipole solitons induced by the repulsive force between adjacent poles, the search for stable multipole solitons with large n is still a challenging problem, while most works were focused on the stability of dipoles and quadrupoles. Very recently, Liu *et al.* predicted that stable multipole solitons can exist in CQ media modulated by a harmonic-Gaussian potential [52]. However, the stability region of necklace-like solitons quickly shrinks with the increase of n , the solitons with $n \geq 8$ being unstable in their entire existence domain.

In this work, we put forward a model admitting the self-trapping of stable multipole solitons with large n . The CQ nonlinearity, combined with an imprinted ring-shaped potential is shown to support two branches of multipole families. The radius of the multipole complexes and the respective value of n can be controlled adjusting the radius of the potential ring. The stability domain for the solitons shrinks *very slowly* with the growth of n , allowing the existence of stable modes with $n > 16$, greatly exceeding values of n that were previously reported for stable multipole solitons. Unstable lower-branch solitons can survive over a long propagation distance, while unstable upper-branch ones are quickly destroyed.

The following presentation is arranged as follows. The model is formulated in Sec. II, and numerical results for static patterns, produced by a systematic numerical analysis, are summarized in Sec. III. Analytical and numerical findings for rotating multipole solitons are reported in Sec. IV. The paper is concluded by Sec. V.

II. MODEL

We consider an optical beam propagating along the z axis in a bulk medium with the CQ nonlinearity and imprinted transverse modulation of the refractive index, which induces the effective radial potential. This setting is governed by the 2D nonlinear Schrödinger equation (NLSE) for the complex field amplitude Ψ , written here in the normalized form

$$i \frac{\partial \Psi}{\partial z} = \left[- \left(\frac{\partial^2}{\partial x^2} + \frac{\partial^2}{\partial y^2} \right) - pV(r) - |\Psi|^2 + |\Psi|^4 \right] \Psi. \quad (1)$$

The effective ring potential, with radius r_0 , radial width d , and depth p , is adopted in the form of a Gaussian whose maximum resides on a circle with a radius r_0

$$V(r) = \exp[-(r - r_0)^2/d^2], \quad (2)$$

where $r = \sqrt{x^2 + y^2}$ [in terms of the similar Gross-Pitaevskii equation (GPE), with z replaced by time t , the potential is $-V(r)$]. Equation (1) conserves the net power (alias the

energy flow) P , angular momentum M , and Hamiltonian H :

$$\begin{aligned} P &= \iint |\psi|^2 dx dy, \\ M &= i \iint \psi^* \left(y \frac{\partial}{\partial x} - x \frac{\partial}{\partial y} \right) \psi dx dy, \\ H &= \iint \left[\left| \frac{\partial \psi}{\partial x} \right|^2 + \left| \frac{\partial \psi}{\partial y} \right|^2 + pV |\psi|^2 \right. \\ &\quad \left. - \frac{1}{2} |\psi|^4 + \frac{1}{3} |\psi|^6 \right] dx dy, \end{aligned} \quad (3)$$

where $*$ stands for the complex conjugate.

Stationary solutions of Eq. (1) are looked for as

$$\Psi(x, y, z) = \psi(x, y) \exp(ibz), \quad (4)$$

where ψ is the soliton's stationary profile and b is the longitudinal propagation constant (in terms of the corresponding GPE, $-b$ is the chemical potential). Substituting ansatz (4) in Eq. (1), we obtain the stationary equation

$$b\psi = \frac{\partial^2 \psi}{\partial x^2} + \frac{\partial^2 \psi}{\partial y^2} + pV\psi + |\psi|^2\psi - |\psi|^4\psi, \quad (5)$$

which can be solved numerically by means of the relaxation or Newton-conjugate-gradient method [2].

Soliton families are defined by propagation constant b , potential depth p , and geometric parameters r_0 and d . By means of scaling, we fix

$$r_0 = 2\pi, \quad (6)$$

and select $d = \sqrt{6}$ and $p = 10$, which makes it possible to produce generic results. Variation of the remaining free parameter b produces families of soliton states which are reported below. Other values of d and r_0 produce quite similar results.

The effective ring-shaped potential is displayed in Fig. 1(a). Note that it is symmetric about the central circle with $r = r_0$, i.e., $V(r = r_0 - r') = V(r = r_0 + r')$ for all $0 < r' < r_0$, see Fig. 1(b). This feature is important for the stabilization of nonlinear modes due to the fact that the fields propagating in the inner and outer annuli ($r < r_0$ and $r > r_0$, respectively) experience the same guidance, in contrast to the case of the harmonic-oscillator trapping potential, which is commonly used to guide optical beams or trap BEC. Potential (2) indeed favors the existence of stable vortex solitons with high topological charges [53], and of stable higher-order solitons with a multiring profile, as shown by additional numerical results.

Before unveiling properties of multipole modes produced by the full nonlinear equation (1), it is instructive to understand the dispersion relation of its linearized counterpart, as linear eigenvalues and eigenmodes essentially affect the build of the nonlinear modes. The linear spectrum produced by the numerical solution of the linearized version of Eq. (5), which is displayed in Fig. 1(c), includes a finite number of discrete real eigenvalues, in addition to the obvious continuous spectrum (not shown here). The growth of the potential depth p results in a shift of the spectrum to the right. The variation of thickness d and radius r_0 also alters the distribution of the eigenvalues. Unlike the system with the harmonic-

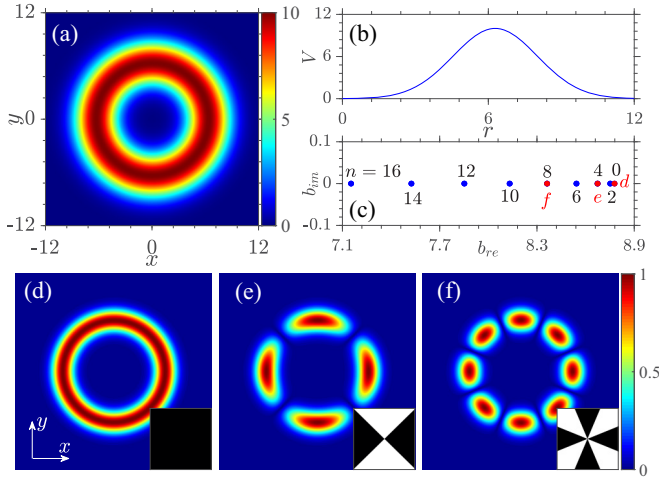


FIG. 1. The (a) top view and (b) radial cross-section of the ring potential (2) with $p = 10$, $r_0 = 2\pi$, $d = \sqrt{6}$. (c) The respective spectrum of real eigenvalues b_{re} produced by the linearized equation (5). The b_{im} denotes the imaginary part of b . The values of n denote the pole number of the linear states from which multipole solitons bifurcate out. (d)–(f) Linear eigenstates of fundamental, quadrupole, and octupole modes corresponding to the eigenvalues marked in (c). Insets in these panels and similar figures displayed below demonstrate the phase structure of the eigenstates (alternation of values 0 and π). All quantities are plotted in dimensionless units.

oscillator potential, the discrete part of the present spectrum is not equidistant. While the lowest (ground-state) eigenvalue is nondegenerate (as it must be, according to the general principles of quantum mechanics), the eigenvalues of the excited states are doubly degenerate, with mutually orthogonal eigenmodes corresponding to pairs of equal eigenvalues. Due to the degeneracy, the eigenmodes with $n \geq 2$ poles correspond to the $(2n - 2)$ th and $(2n - 1)$ th eigenvalues, while the first eigenvalue corresponds to the ground-state eigenmode shown in Fig. 1(d). A linear superposition of the two degenerate eigenmodes also produces an allowed state of the linear system. For example, two superpositions of two orthogonal dipole modes (i.e., those oriented along x and y directions), with $n = 2$, build two counterrotating vortex states, which carry the angular momentum and opposite winding numbers (topological charges) $m = \pm 1$.

III. NUMERICAL RESULTS FOR STATIC MULTIPOLE SOLITONS

Bearing the linear case in mind, we now focus on the properties of multipole-mode solitons. First, dipole solitons bifurcate from the linear eigenstates corresponding to the coinciding (mutually degenerate) second and third eigenvalues, $b = 8.753$, which are shown in Fig. 1(c). The power and amplitude initially increase with the growth of propagation constant b , see the short bottom branch in the inset to Fig. 2(c). As b increases to 8.903, the peak value of the dipole soliton attains value $|\psi|_{\max} = 1$ (in the scaled notation adopted here). Thus, the nonlinearity experienced by the dipole solitons is entirely focusing at $b < 8.903$. At $b > 8.903$ ($|\psi|_{\max} > 1$), the effect of the quintic defocusing becomes dominant in the core

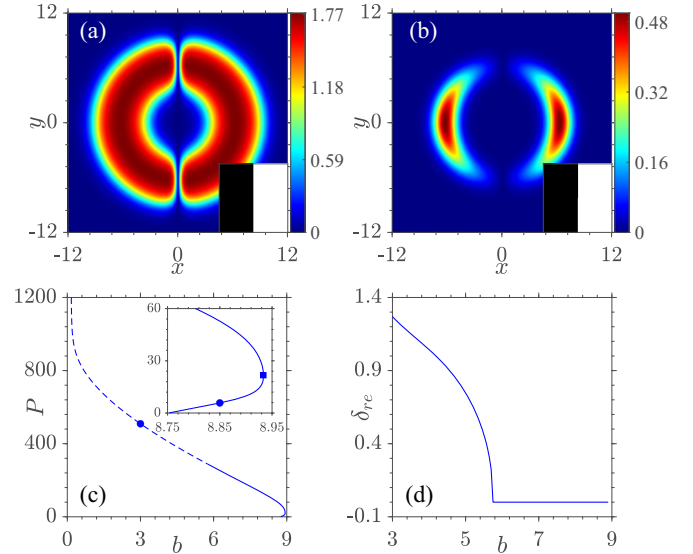


FIG. 2. (a), (b) $|\psi(x, y)|$ for the unstable upper-branch and stable lower-branch dipole solitons with $b = 3.0$ and $b = 8.85$, which are marked by circles in the main plot and inset in (c), respectively. Insets in (a) and (b) show the corresponding simple phase distribution in the dipole modes. (c) Power of the dipole solitons P versus propagation constant b . Inset: Zoom of the $P(b)$ curve near the turning point. The square denotes the merging point (cutoff of b). The solid and dashed lines denote, severally, stable and unstable segments of the dipole-soliton families. (d) The instability growth rate δ_{re} (real part of δ) versus b for the upper-branch dipole solitons. Parameters are $p = 10$, $r_0 = 2\pi$, $d = \sqrt{6}$ in all the panels. All quantities are plotted in dimensionless units.

region with $|\psi(x, y)| > 1$. The defocusing nonlinearity in the core region arrests the growth of $|\psi|_{\max}$ and accelerates the increase of the soliton's width, defined as

$$W^2 \equiv \iint (x^2 + y^2) \psi^2 dx dy / P. \quad (7)$$

The gradual transition to the defocusing nonlinearity, along with the action of the trapping potential, prevents the existence of dipole solitons for the propagation constant exceeding a cutoff value, viz., at $b > b_{\text{cut}} = 8.933$, the corresponding power being $P = 21.693$. Instead, further increase of P is accommodated by the top branch of the $P(b)$ dependence in Fig. 2(c), with the negative slope, $dP/db < 0$, which continues the short bottom branch through the turning point, $b > b_{\text{cut}}$.

Dipole solitons belonging to the lower branch in Fig. 2(c) are composed of two far-separated crescent-shaped lobes with opposite signs, tightly attached to the potential ring [Fig. 2(b)]. With the increase of b , the crescent lobes elongate, becoming thinner, while their amplitude grows under the action of the dominant cubic focusing nonlinearity. On the other hand, the dipole solitons belonging to the upper branch in Fig. 2(c) are shaped mainly by the dominant defocusing quintic nonlinearity, which results in the expansion of the lobes along the radial and azimuthal directions. As a result, the two lobes with opposite signs are separated by narrow fissures, rather than wide gaps, see Fig. 2(b). The expansion

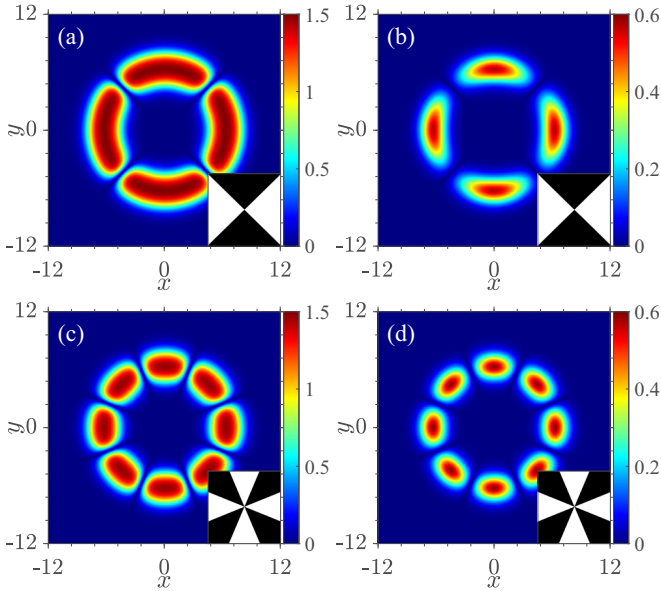


FIG. 3. (a), (b) $|\psi(x, y)|$ for stable upper-branch and unstable lower-branch quadrupole solitons with $b = 7.0$ and $b = 8.8$, respectively, which are marked in Fig. 4(a). (c), (d) The same for upper- and lower-branch stable and unstable octupole solitons with $b = 7.2$ and $b = 8.5$, respectively, which are marked in Fig. 4(b). All quantities are plotted in dimensionless units.

is more salient for solitons with higher power, which tend to develop a flat-top profile.

The stability of the stationary states can be analyzed by taking perturbed solutions to Eq. (1) as

$$\Psi(x, y, z) = [\psi(x, y) + f(x, y) \exp(\delta z) + g^*(x, y) \exp(\delta^* z)] \exp(ibz), \quad (8)$$

where f and g are infinitesimal perturbations and δ is the instability growth rate. The linearization of Eq. (1) around ψ leads to an eigenvalue problem for $f(x, y)$ and $g(x, y)$:

$$i \begin{bmatrix} \mathcal{M}_1 & \mathcal{M}_2 \\ -\mathcal{M}_2^* & -\mathcal{M}_1^* \end{bmatrix} \begin{bmatrix} f \\ g \end{bmatrix} = \delta \begin{bmatrix} f \\ g \end{bmatrix}. \quad (9)$$

Here, $\mathcal{M}_1 \equiv \frac{\partial^2}{\partial x^2} + \frac{\partial^2}{\partial y^2} + pV - b + 2|\psi|^2 - 3|\psi|^4$, $\mathcal{M}_2 \equiv \psi^2(1 - 2|\psi|^2)$, and $*$ denotes the complex conjugate. Equations (9) can be solved by means of the Fourier collocation method [2]. Solitons are stable if all eigenvalues δ are imaginary.

Instability growth rates for the upper- and lower-branch dipole solitons were obtained from the numerical solutions of Eqs. (9). The results demonstrate that the lower branch is stable in its entire existence domain, while the upper branch is stable if the propagation constant exceeds a certain critical value (which is a generic feature of 2D NLSEs with the CQ nonlinearity), viz., $b > b_{\text{cr}} = 5.751$ [see Fig. 2(c)]. At $b < b_{\text{cr}}$, the instability growth rate rapidly increases with the decrease of b , see Fig. 2(d).

Next, we address multipole-mode solitons with a larger number n of the lobes. The patterns of $|\psi(x, y)|$ for quadrupole and octupole solitons are shown in Fig. 3. Similar to the dipoles, the lobes forming the lower-branch

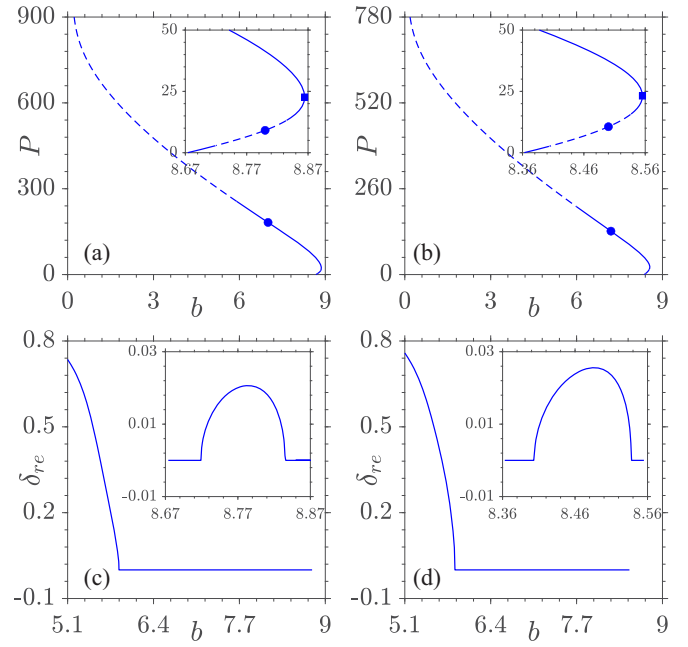


FIG. 4. (a), (b) Integral power P versus propagation constant b for quadrupole and octupole solitons, respectively. Insets: The $P(b)$ curves near the merging (turning) point. Solid and dashed lines denote stable and unstable solitons. (c), (d) The instability growth rate δ_{re} versus b for the upper-branch and lower-branch (inset) quadrupole and octupole solitons, respectively. All quantities are plotted in dimensionless units.

quadrupoles are separated by relatively wide fissures [Fig. 3(b)], while the lobes of their upper-branch counterparts are “fatter,” being tightly packed along the potential ring [see Fig. 3(a)]. These features indicate that the repulsion between adjacent lobes of the upper-branch quadrupoles is strong.

Adjacent lobes of octupole solitons are pressed onto each other tighter than in the quadrupoles, cf. Figs. 3(b) and 3(c). Due to the confinement imposed by the annular (ring-shaped) potential, the radial size of the multipole solitons (the distance from the center of each lobe to the origin) does not change with the growth of n . As mentioned above, the adjacent lobes in all multipole solitons have alternating signs, see inset phase plots in Fig. 3.

The lower $P(b)$ branch for the quadrupole solitons, originating from the linear mode at $b = 8.674$, merges with the upper branch at $b_{\text{cut}} = 8.864$ [see Fig. 4(a)]. The merging (turning) point for the octupole solitons is $b_{\text{cut}} = 8.555$, see Fig. 4(b). The shift of b_{cut} for solitons with different numbers of poles is a straightforward consequence of the difference in the linear eigenvalues of b from which the lower-branch solitons bifurcate. The upper $P(b)$ curves can extend to still larger values of P for smaller b . We do not pay more attention to the corresponding multipole solitons as they are definitely unstable.

Unlike the dipole solitons which are completely stable on the lower branch [see Fig. 2(c)], weak instability occurs for the lower-branch quadrupole and octupole solitons, as seen in insets in Figs. 4(a) and 4(b). The instability region expands slowly with the growth of the pole number, as seen in insets to Figs. 4(c), 4(d), and 5(d). Further, the upper-branch

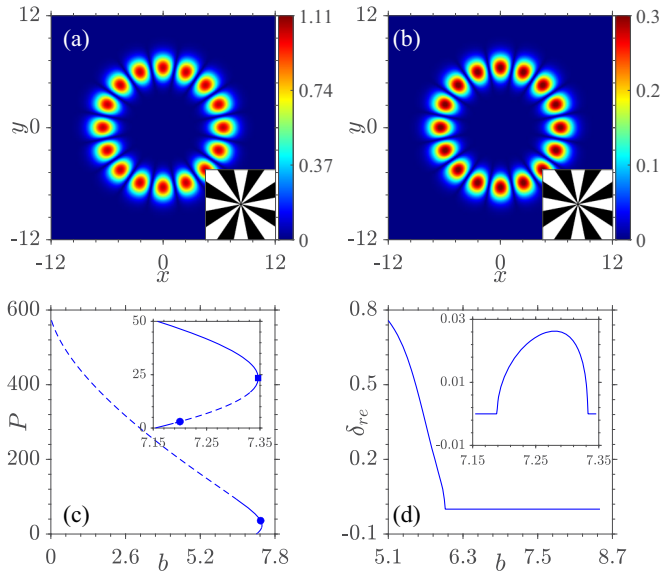


FIG. 5. (a), (b) $|\psi(x, y)|$ of 16-pole solitons with $b = 7.3$ and 7.2 , which are marked, respectively, in the main plot and inset in (c). Insets in (a) and (b) show the corresponding phase distribution. (c) The $P(b)$ dependence for the 16-pole solitons. Inset: The $P(b)$ curve near the merger (turning) point. The solid and dashed lines denote stable and unstable segments of the soliton families, respectively. (d) The instability growth rate δ_{re} versus b for the upper branch and lower branch (inset) of the 16-dipole soliton family. All quantities are plotted in dimensionless units.

quadrupole and octupole solitons are stable, severally, in intervals $b \in [6.013, 8.864]$ and $b \in [5.859, 8.555]$, as shown in Figs. 4(c) and 4(d). With the increase of n , the stability segment of the upper-branch multipole solitons shrinks *very slowly*, which is the most important finding of this work. For example, the width of the stability intervals for the quadrupoles and octupoles are 2.851 and 2.696, respectively. Actually, these intervals, located to the left of the merging point b_{cut} , are relatively large ones. We stress that the stability of the multipole solitons trapped in the annular potential is very different from that for vortex solitons trapped in the same potential [53], where the lower-branch vortices with all topological charges are unstable in their almost entire existence domain, while all upper-branch vortices are completely stable.

To further understand the properties of multipole solitons, we investigated necklace-shaped ones with $n = 10, 12, 14$, and 16. Representative examples of the necklaces with $n = 16$ poles are presented in Figs. 5(a) and 5(b). Due to the confinement imposed by the annular potential, the components in both lower- and upper-branch solitons are tightly packed in the azimuthal direction and somewhat stretched along the radius. This effect is more evident for the solitons with a higher power or higher n . The lower-branch necklace solitons with $n = 16$ bifurcate from the linear mode at $b = 7.154$, while the point of the merger of the lower and upper branches is at $b_{cut} = 7.346$. The stronger repulsion between the adjacent lobes in the case of larger n causes shrinkage of the stability interval for the upper-branch solitons. Nevertheless, for $n = 16$ there still exists a sufficiently wide stability interval to the left of b_{cut} , see Fig. 5(d). A nonvanishing stability region can be found

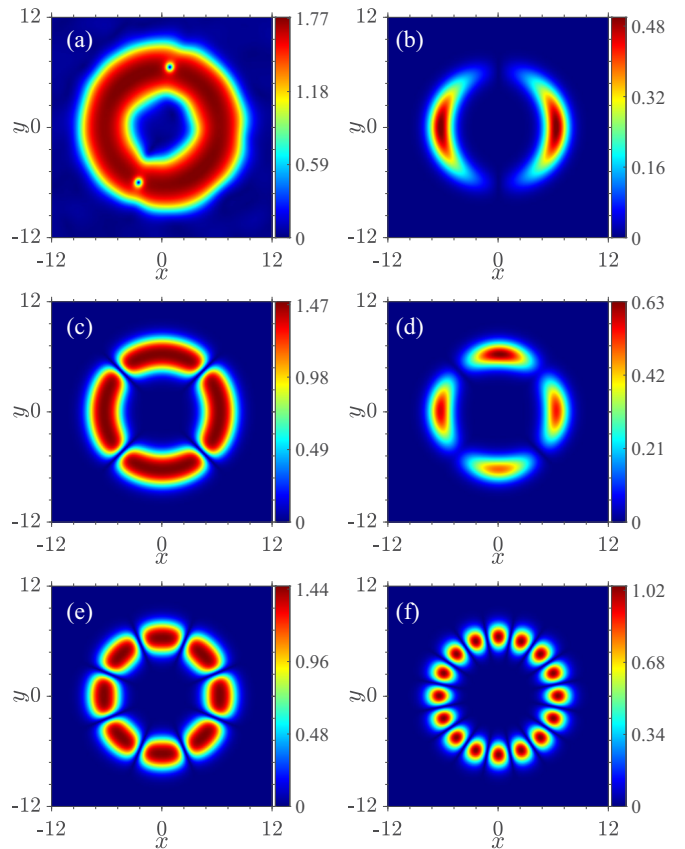


FIG. 6. Examples of the simulated propagation of (a), (d) unstable and (b), (c), (e), and (f) stable solitons with (a), (b) $n = 2$, (c), (d) $n = 4$, (e) $n = 8$, and (f) $n = 16$. The solitons belong to the lower branch in (b), (d) and to the upper branch in other panels. The propagation constant is $b = 3.0$ in (a), 8.85 in (b), 7.0 in (c), 8.8 in (d), 7.2 in (e), and 7.3 in (f). The panels exhibit the outcome of the propagation after passing the distance $z = 100$ in (a), 1540 in (d), and 2000 in the other panels. All quantities are plotted in dimensionless units.

for still higher values of n (e.g., $n = 20$). These findings are in sharp contrast to the in 2D cubic-quintic NLSE with the harmonic-Gaussian potential [52], where the stability region is virtually invisible for $n > 8$. We also note that the main results hold for multipole solitons with different numbers of poles in potentials with varying depths p . The stability region gradually shrinks with the decrease of p due to weakening of the trapping.

To verify the predictions of the linear-stability analysis for the multipole families with different values of n , we conducted extensive simulations of perturbed propagation for the solitons, by means of the split-step Fourier method. The perturbation was added, as white noise, to the input at $z = 0$ for stable solitons and no perturbations were added to the solitons whose instability was predicted by the computation of eigenvalues for small perturbations. Typical examples of stable and unstable propagation are presented in Fig. 6. For the upper-branch dipole soliton with $b = 3.0$, the large instability growth rate $\delta_{re} = 1.266$ destroys the original pattern, shown in Fig. 2(a), after a short propagation distance, see Fig. 6(a). The lower-branch quadrupole soliton with $b = 8.8$ and a small

instability growth rate, $\delta_{re} = 0.019$, is only deformed, but not destroyed, after a long distance [Fig. 6(d)]. White noise added to the stable solitons is quickly radiated away in Figs. 6(b), 6(d) to 6(f). The agreement between the predictions of the linear-stability analysis and direct simulations is obtained for all the cases considered.

IV. ROTATING MULTIPOLE SOLITONS: ANALYTICAL AND NUMERICAL RESULTS

Because the multipole solitons have the articulate structure in the azimuthal direction, it is natural to try setting them in rotation, by imprinting a phase torque

$$\psi(x, y) \rightarrow \psi(x, y) \exp(im\theta), \quad (10)$$

with integer index m , onto the static soliton. First, the result of the application of this “crank” to the static multipole with the narrow radial shape can be predicted in an approximate analytical form. Indeed, assuming that the result is a pattern rotating with angular velocity Ω , in the form of

$$\Psi(x, y, z) = \varphi(r, \theta - \Omega z) \exp(ibz + im\theta) \quad (11)$$

[cf. Eq. (4)], which is written in the polar coordinates (r, θ) , we substitute ansatz (11) in the underlying equation (1). This leads to the conclusion that wave function φ satisfies the stationary equation

$$b\varphi = \frac{\partial^2 \varphi}{\partial r^2} + \frac{1}{r} \frac{\partial \varphi}{\partial r} + \frac{1}{r^2} \frac{\partial^2 \varphi}{\partial \tilde{\theta}^2} + \left[pV(r) - \frac{m^2}{r^2} \right] \varphi + |\varphi|^2 \varphi - |\varphi|^4 \varphi \quad (12)$$

[cf. Eq. (5)], where $\tilde{\theta} \equiv \theta - \Omega z$, the term $-m^2/r^2$ representing the centrifugal energy. An additional relation produced by the substitution of ansatz (11) in Eq. (1) is an *approximate* one, $\Omega = 2m/r^2$. It is approximate because it produces Ω as a function of r , while the angular velocity must be a constant. However, for the pattern confined to a narrow annulus around $r = r_0$, one may, in the first approximation, replace r by r_0 , thus predicting the angular velocity and respective rotation period

$$\Omega \approx 2m/r_0^2, \quad Z = 2\pi/\Omega \approx \pi m^{-1} r_0^2. \quad (13)$$

In particular, for the radial size $r_0 = 2\pi$ of the trap adopted here [see Eq. (6)] and $m = 1$, Eq. (13), predicts the rotation period $Z \approx 4\pi^3 \approx 124$, while the value produced by direct simulations is $Z \approx 120$ (see below), hence the approximation is quite accurate. Furthermore, the simulation for the torque with $m = 2$ produces the rotation with the double angular velocity, in agreement with prediction given by Eq. (13).

The competition of the centrifugal energy with the trapping potential in Eq. (12) may eventually suppress the trapping effect if the effective combined potential, $-pV(r) + m^2/r^2$, has no minimum. In the lowest approximation, the condition for the survival of the minimum is

$$r_0^3 > \sqrt{2em^2 d/p}. \quad (14)$$

Systematic simulations clearly confirm transition to a regime of steady rotation, initiated by the application of torque (10). The rotation lasts for indefinitely many periods, without

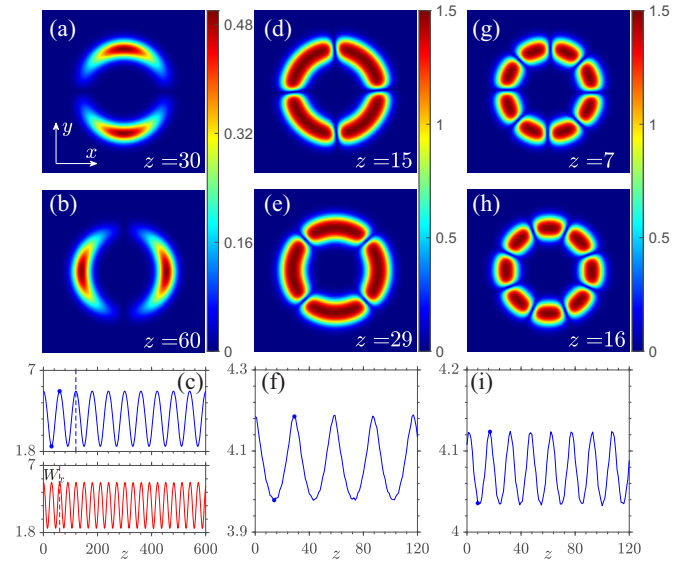


FIG. 7. The stable counterclockwise rotation of (a)–(c) dipole, (d)–(f) quadrupole, and (g)–(i) octupole solitons initiated by torque (10) with $m = 1$, applied to inputs selected as the stationary solitons presented in Figs. 6(b), 6(c) and 6(e), respectively. The periods of oscillations of the x width observed in panels (c), (f), and (i) agree with the prediction Z/n , see the main text. The lower plot in (c) displays the oscillations of the x width of the same dipole soliton initiated by the double torque, with $m = 2$. In panel (c), the vertical dashed lines define one rotation period, Z . All quantities are plotted in dimensionless units.

generating any tangible loss (see Fig. 7). In particular, the torque with $m = 1$ gives rise to the robust rotational state with period $Z \approx 120$.

The rotation is coupled to periodic oscillations of the effective soliton’s width. In particular, the oscillations of the width in the x direction, defined by

$$W_x^2 \equiv \iint x^2 \psi^2 dx dy / P \approx W^2 / 2 \quad (15)$$

[cf. Eq. (7)], with period $Z \approx 120$, initiated by the torque with $m = 1$ in Eq. (10), are plotted in Figs. 7(c), 7(f), and 7(i) for the rotating dipole, quadrupole, and octupole, respectively. Note that the period of oscillations of width (15) exhibited by an n multipole rotating with period Z is Z/n . The oscillations observed in Figs. 7(c), 7(f) and 7(i) completely agree with this expectation.

To illustrate the steady rotation, examples of the patterns are displayed at $z = Z/4$ and $Z/2$ for the dipole soliton [Figs. 7(a) and 7(b)], $Z/8$ and $Z/4$ for the quadrupole [Figs. 7(d) and 7(e)], and $Z/16$ and $Z/8$ for the octupole [Figs. 7(g) and 7(h)]. The robustness of the rotation is corroborated, in particular, by Fig. 7(c), which shows an example of long evolution, for $z = 600$ (around five full rotation periods). Movies presented in the Supplemental Material [54] illustrate the rotation dynamics in full detail (the third movie displays the clockwise rotation, while others represent the opposite direction). Robust rotary states of the multispot patterns suggest new possibilities for all-optical routing of weak data-carrying light beams [45].

The multipole solitons predicted in this work can be created in the currently available optical experimental setups. In particular, polydiacetylene paratoluene sulfonate (PPS) exhibits competing nonlinearities with sufficiently large cubic and quintic indices [20]. For a beam with carrier wavelength $\lambda = 1.6 \mu\text{m}$, the second- and fourth-order optical indices are $n_2 = 2.2 \times 10^{-3} \text{ cm}^2/\text{GW}$ and $n_4 = 0.8 \times 10^{-3} \text{ cm}^4/\text{GW}^2$, respectively. The critical intensity at which $\delta n = 0$ is $I_0 = |n_2/n_4| = 2.75 \text{ GW/cm}^2$. This material exhibits focusing nonlinearity at $I < 0.5I_0$ and becomes defocusing at $I > 0.5I_0$. In other words, a localized beam experiences self-defocusing around the peak intensity (assuming $I_{\text{max}} > 0.5I_0$) and focusing in the wings, where $I < 0.5I_0$. As concerns the linear refractive-index modulation inducing the annular trapping potential, it may be created by means of the well-elaborated technology used for the production of multilayer fibers [55].

V. CONCLUSION

Summarizing, we investigated the existence, stability, and propagation dynamics of excited nonlinear states containing different even numbers n of lobes in CQ (cubic-quintic) optical media equipped with an annular (ring-shaped) trapping potential. Adjacent components of such solitons have

opposite signs, being uniformly placed along the potential annulus. With the increase of the soliton's amplitude, the transition from focusing to defocusing nonlinearity, along with the action of the trapping potential, gives rise to two branches of multipole soliton families, with opposite slopes of the power-versus-propagation-constant curves. With the increase of n , the stability domain of the solitons shrinks very slowly, allowing the tangible presence of stable solitons with $n > 16$. Steady rotation of multipole solitons, initiated by the application of the phase torque, is predicted analytically and numerically. The results suggest new ways of manipulating light signals and the creation of novel self-trapped states. The analysis reported here can be generalized for optical solitons in competing quadratic-cubic media, matter-wave solitons in Bose-Einstein condensates, and quantum droplets in Bose-Bose mixtures trapped in a ring potential. A challenging possibility is to extend the consideration for elliptically shaped trapping potentials.

ACKNOWLEDGMENTS

This work is supported by the Natural Science Basic Research Plan in Shaanxi Province of China (Grant No. 2022JZ-02) and Israel Science Foundation (Grant No. 1695/22).

-
- [1] Y. S. Kivshar and G. P. Agrawal, *Optical Solitons: From Fibers to Photonic Crystals* (Academic, New York, 2003).
- [2] J. Yang, *Nonlinear Waves in Integrable and Nonintegrable Systems* (SIAM, Philadelphia, 2010).
- [3] B. A. Malomed, *Multidimensional Solitons* (AIP, Melville, NY, 2022).
- [4] W. Krolikowski, E. A. Ostrovskaya, C. Weinau, M. Geisser, G. McCarthy, Y. S. Kivshar, C. Denz, and B. Luther-Davies, Observation of dipole-mode vector solitons, *Phys. Rev. Lett.* **85**, 1424 (2000).
- [5] L. Ge, Q. Wang, M. Shen, and J. Shi, Dipole solitons in nonlocal nonlinear media with anisotropy, *Opt. Commun.* **284**, 2351 (2011).
- [6] J. Yang, I. Makasyuk, A. Bezryadina, and Z. Chen, Dipole and quadrupole solitons in optically induced two-dimensional photonic lattices: theory and experiment, *Stud. Appl. Math.* **113**, 389 (2004).
- [7] T. Zang, M. Shen, and L. Ge, Stability of quadrupole solitons in nonlocal media, *Optik* **227**, 166052 (2021).
- [8] D. Mihalache, D. Mazilu, L.-C. Crasovan, B. A. Malomed, F. Lederer, and L. Torner, Robust soliton clusters in media with competing cubic and quintic nonlinearities, *Phys. Rev. E* **68**, 046612 (2003).
- [9] L. Dong, H. Wang, W. Zhou, X. Yang, X. Lv, and H. Chen, Necklace solitons and ring solitons in Bessel optical lattices, *Opt. Express* **16**, 5649 (2008).
- [10] N. B. Aleksić, A. I. Strinić, M. M. Petroski, and M. S. Petrović, Necklace beams in media with cubic-quintic nonlinearity, *Opt. Quant. Electron* **52**, 73 (2020).
- [11] P. Li, B. A. Malomed, and D. Mihalache, Metastable soliton necklaces supported by fractional diffraction and competing nonlinearities, *Opt. Express* **28**, 34472 (2020).
- [12] L. Dong, D. Liu, W. Qi, L. Wang, H. Zhou, P. Peng, and C. Huang, Necklace beams carrying fractional angular momentum in fractional systems with a saturable nonlinearity, *Commun. Nonlinear Sci.* **99**, 105840 (2021).
- [13] L. Zeng and J. Zeng, Preventing critical collapse of higher-order solitons by tailoring unconventional optical diffraction and nonlinearities, *Commun. Phys.* **3**, 26 (2020).
- [14] Q. Wang, L. Zhang, and L. Ke, Parameters controlling of vortex solitons in nonlocal nonlinear medium with gradually characteristic length, *Chaos, Solitons and Fractals* **161**, 112319 (2022).
- [15] D. Liu, Y. Gao, D. Fan, and L. Zhang, Higher-charged vortex solitons in harmonic potential, *Chaos, Solitons and Fractals* **171**, 113422 (2023).
- [16] D. Mihalache, D. Mazilu, L.-C. Crasovan, I. Towers, B. A. Malomed, A. V. Buryak, L. Torner, and F. Lederer, Stable three-dimensional spinning optical solitons supported by competing quadratic and cubic nonlinearities, *Phys. Rev. E* **66**, 016613 (2002).
- [17] M. Quiroga-Teixeiro and H. Michinel, Stable azimuthal stationary state in quintic nonlinear optical media, *J. Opt. Soc. Am. B* **14**, 2004 (1997).
- [18] V. I. Berezhiani, V. Skarka, and N. B. Aleksić, Dynamics of localized and nonlocalized optical vortex solitons in cubic-quintic nonlinear media, *Phys. Rev. E* **64**, 057601 (2001).
- [19] H. Michinel, J. R. Salgueiro, and M. J. Paz-Alonso, Square vortex solitons with a large angular momentum, *Phys. Rev. E* **70**, 066605 (2004).
- [20] B. L. Lawrence and G. I. Stegeman, Two-dimensional bright spatial solitons stable over limited intensities and ring formation in polydiacetylene para-toluene sulfonate, *Opt. Lett.* **23**, 591 (1998).

- [21] A. S. Reyna and C. B. de Araújo, High-order optical nonlinearities in plasmonic nanocomposites – a review, *Adv. Opt. Photon.* **9**, 720 (2017).
- [22] A. S. Reyna, K. C. Jorge, and C. B. de Araújo, Two-dimensional solitons in a quintic-septimal medium, *Phys. Rev. A* **90**, 063835 (2014).
- [23] V. E. Zakharov, V. V. Sobolev, and V. C. Synakh, Behavior of light beams in nonlinear media, *Sov. Phys. JETP* **33**, 77 (1971).
- [24] C. Josserand and S. Rica, Coalescence and droplets in the subcritical nonlinear Schrödinger equation, *Phys. Rev. Lett.* **78**, 1215 (1997).
- [25] M. Soljačić, S. Sears, and M. Segev, Self-trapping of “necklace beams” in self-focusing Kerr media, *Phys. Rev. Lett.* **81**, 4851 (1998).
- [26] M. Soljačić and M. Segev, Self-trapping of “necklace-ring” beams in self-focusing Kerr media, *Phys. Rev. E* **62**, 2810 (2000).
- [27] A. S. Desyatnikov, D. Neshev, E. A. Ostrovskaya, Y. S. Kivshar, W. Krolikowski, B. Luther-Davies, J. J. García-Ripoll, and V. M. Pérez-García, Multipole spatial vector solitons, *Opt. Lett.* **26**, 435 (2001).
- [28] A. S. Desyatnikov, D. Neshev, E. A. Ostrovskaya, Y. S. Kivshar, G. McCarthy, W. Krolikowski, and B. Luther-Davies, Multipole composite spatial solitons: Theory and experiment, *J. Opt. Soc. Am. B* **19**, 586 (2002).
- [29] M. Soljačić and M. Segev, Integer and fractional angular momentum borne on self-trapped necklace-ring beams, *Phys. Rev. Lett.* **86**, 420 (2001).
- [30] Y. V. Kartashov, L.-C. Crasovan, D. Mihalache, and L. Torner, Robust propagation of two-color soliton clusters supported by competing nonlinearities, *Phys. Rev. Lett.* **89**, 273902 (2002).
- [31] D. Mihalache, D. Mazilu, L. C. Crasovan, B. A. Malomed, F. Lederer, and L. Torner, Soliton clusters in three-dimensional media with competing cubic and quintic nonlinearities, *J. Opt. B: Quantum Semiclass. Opt.* **6**, S333 (2004).
- [32] T. D. Grow, A. A. Ishaaya, L. T. Vuong, and A. L. Gaeta, Collapse and stability of necklace beams in Kerr media, *Phys. Rev. Lett.* **99**, 133902 (2007).
- [33] C. Rotschild, M. Segev, Z. Xu, Y. V. Kartashov, L. Torner, and O. Cohen, Two-dimensional multipole solitons in nonlocal nonlinear media, *Opt. Lett.* **31**, 3312 (2006).
- [34] Y. V. Kartashov, B. A. Malomed, and L. Torner, Solitons in nonlinear lattices, *Rev. Mod. Phys.* **83**, 247 (2011).
- [35] J. Yang, I. Makasyuk, A. Bezryadina, and Z. Chen, Dipole solitons in optically induced two-dimensional photonic lattices, *Opt. Lett.* **29**, 1662 (2004).
- [36] Y. V. Kartashov and L. Torner, Multipole-mode surface solitons, *Opt. Lett.* **31**, 2172 (2006).
- [37] L. Dong and H. Li, Surface solitons in nonlinear lattices, *J. Opt. Soc. Am. B* **27**, 1179 (2010).
- [38] J. Yang, I. Makasyuk, P. G. Kevrekidis, H. Martin, B. A. Malomed, D. J. Frantzeskakis, and Z. Chen, Necklacelike solitons in optically induced photonic lattices, *Phys. Rev. Lett.* **94**, 113902 (2005).
- [39] P. Rose, T. Richter, B. Terhalle, J. Imbrock, F. Kaiser, and C. Denz, Discrete and dipole-mode gap solitons in higher-order nonlinear photonic lattices, *Appl. Phys. B* **89**, 521 (2007).
- [40] H. Susanto, K. J. H. Law, P. G. Kevrekidis, L. Tang, C. Lou, X. Wang, and Z. Chen, Dipole and quadrupole solitons in optically-induced two-dimensional defocusing photonic lattices, *Physica D* **237**, 3123 (2008).
- [41] S. Xia, D. Song, L. Tang, C. Lou, and Y. Li, Self-trapping and oscillation of quadruple beams in high band gap of 2d photonic lattices, *Chin. Opt. Lett.* **11**, S10503 (2013).
- [42] H. Wang, S. Shi, X. Ren, X. Zhu, B. A. Malomed, D. Mihalache, and Y. He, Two-dimensional solitons in triangular photonic lattices with parity-time symmetry, *Opt. Commun.* **335**, 146 (2015).
- [43] H. Wang, X. Ren, J. Huang, and Y. Weng, Evolution of vortex and quadrupole solitons in the complex potentials with saturable nonlinearity, *J. Opt.* **20**, 125504 (2018).
- [44] Y. V. Kartashov, B. A. Malomed, V. A. Vysloukh, and L. Torner, Stabilization of multibeam necklace solitons in circular arrays with spatially modulated nonlinearity, *Phys. Rev. A* **80**, 053816 (2009).
- [45] Y. V. Kartashov, R. Carretero-González, B. A. Malomed, V. A. Vysloukh, and L. Torner, Multipole-mode solitons in Bessel optical lattices, *Opt. Express* **13**, 10703 (2005).
- [46] L. Dong, J. Wang, H. Wang, and G. Yin, Bessel lattice solitons in competing cubic-quintic nonlinear media, *Phys. Rev. A* **79**, 013807 (2009).
- [47] W.-P. Hong, Surface multipole solitons on photorefractive media with Bessel optical lattices, *J. Korean Phys. Soc.* **66**, 919 (2015).
- [48] B. B. Baizakov, B. A. Malomed, and M. Salerno, Matter-wave solitons in radially periodic potentials, *Phys. Rev. E* **74**, 066615 (2006).
- [49] C. Huang, Y. Ye, S. Liu, H. He, W. Pang, B. A. Malomed, and Y. Li, Excited states of two-dimensional solitons supported by the spin-orbit coupling and field-induced dipole-dipole repulsion, *Phys. Rev. A* **97**, 013636 (2018).
- [50] Y. V. Kartashov, B. A. Malomed, and L. Torner, Metastability of quantum droplet clusters, *Phys. Rev. Lett.* **122**, 193902 (2019).
- [51] L. Dong, D. Liu, Z. Du, K. Shi, and W. Qi, Bistable multipole quantum droplets in binary Bose-Einstein condensates, *Phys. Rev. A* **105**, 033321 (2022).
- [52] D. Liu, Y. Gao, D. Fan, and L. Zhang, Multi-stable multipole solitons in competing nonlinearity media, *Chaos Solitons & Fractals* **173**, 113691 (2023).
- [53] L. Dong, M. Fan, and B. A. Malomed, Stable higher-charge vortex solitons in the cubic-quintic medium with a ring potential, *Opt. Lett.* **48**, 4817 (2023).
- [54] See Supplemental Material at <http://link.aps.org/supplemental/10.1103/PhysRevA.108.063501> for movies.
- [55] C. Y. H. Tsao, D. N. Payne, and W. A. Gambling, Model characteristics of 3-layered optical fiber wave-guides—a modified approach, *J. Opt. Soc. Am. A* **6**, 555 (1989).